

## Supporting Information for

# Synthesis, structure and optical properties of Zr(IV)- and Ce(IV)-based CAU-24 with 1,2,4,5-tetrakis(4-carboxyphenyl)benzene

M. Lammert,<sup>a</sup> H. Reinsch,<sup>a</sup> C. A. Murray,<sup>b</sup> M. T. Wharmby,<sup>b</sup> H. Terraschke<sup>a</sup> and N. Stock<sup>a</sup>

<sup>a</sup> Institut für Anorganische Chemie, Christian-Albrechts-Universität zu Kiel, Max-Eyth-Straße 2, 24118 Kiel, Germany. E-mail: stock@ac.uni-kiel.de

<sup>b</sup> Diamond Light Source Ltd., Diamond House, Harwell Science & Innovation Campus, Didcot, Oxfordshire, OX11 0DE, UK. E-mail: michael.wharmby@diamond.ac.uk

<b>1. Synthesis procedures</b>	<b>2</b>
<b>2. Powder X-ray diffraction</b>	<b>9</b>
<b>3. Thermal analysis</b>	<b>16</b>
<b>4. IR spectroscopy</b>	<b>20</b>
<b>5. NMR spectroscopy</b>	<b>21</b>
<b>6. N<sub>2</sub> sorption measurement</b>	<b>23</b>
<b>7. Luminescence measurements</b>	<b>24</b>

## 1. Synthesis procedure

### Materials and Methods.

Cerium ammonium nitrate (98 %,  $(\text{NH}_4)_2\text{Ce}(\text{NO}_3)_6$ , Alfa Aesar), Zirconium(IV) dinitrate oxide hydrate (98%,  $\text{ZrO}(\text{NO}_3)_2 \cdot \text{H}_2\text{O}$ , ABCR), 1,2,4,5-Tetrakis(4-carboxyphenyl)benzene (98%, H<sub>4</sub>TCPB, Sigma Aldrich).

PXRD experiments for product identification were performed on a STOE Stadi P Combi diffractometer with MoK<sub>α1</sub> radiation equipped with a Mythen 2 1K detector system and an xy-stage. The high resolution PXRD patterns were recorded on a Stadi P diffractometer with CuK<sub>α1</sub> radiation using a Mythen 2 1K detector. For temperature dependent X-ray diffraction measurements, the STOE Stadi P Combi diffractometer with MoK<sub>α1</sub> radiation equipped with a Mythen 2 1K detector system was equipped with a capillary furnace. These measurements were carried out under air in a 0.5 mm quartz capillary in a range of 1-19° 2θ with a measuring time of 3 min for each 5 °C temperature step.

NMR spectra were measured on a Bruker DRX 200 spectrometer. Sorption experiments were performed using a BEL Japan Inc. Belsorpmax. The specific surface areas were determined using the Rouquerol approach and the micropore volume was calculated at p/p<sub>0</sub> = 0.5. IR spectra were measured on a Bruker ALPHA-FT-IR A220/D-01 spectrometer equipped with an ATR unit. Thermogravimetric measurements were performed on a TA instruments Q500 under air flow (10 ml min<sup>-1</sup>) with a heating rate of 4 K min<sup>-1</sup>.

The luminescence measurements have been performed at room temperature with a HORIBA Jobin Yvon GmbH fluorescence spectrometer (Fluorolog3) equipped with a iHR-320-FA Triple Grating Imaging spectrograph, a Syncerity CCD detector and a 450 W xenon lamp. Colour coordinates have been calculated from the measured emission spectra applying the Spectra Lux Software v.2.0.<sup>[1]</sup> The reflection spectra of the powdered sample was recorded also at room temperature with a Varian Techtron Pty. UV/Vis/NIR two-channel Cary 5000 spectrometer, applying BaSO<sub>4</sub> as reference material.

**Details of Data Collection.** As synthesized samples were loaded into 0.5 mm borosilicate glass capillary tubes, which were then flame sealed. Activated materials were loaded into 0.5 mm quartz glass capillary tubes and heated at 140 °C for 3 hours under dynamic vacuum ( $10^{-2}$  kPa) before also being flame sealed. Samples were mounted on the high-resolution powder X-ray diffraction beamline at beamline I11 (Diamond Light Source, Oxon., UK) and data were collected using monochromatic X-rays ( $\lambda = 0.826215$  Å) in Debye-Scherrer geometry with the Mythen detector.<sup>[2]</sup> Four datasets at different δ-circle values (2.00°, 2.25°, 2.50° and 2.75°) were collected to allow corrections for the gaps between detector plates to

be applied. These datasets were merged to give a final dataset with a range of 2.1-92.6° 2θ and a step size of 0.05° 2θ. For Rietveld refinement, only the range 2-30° 2θ was considered.

Sample treatment prior to NMR measurements: Solution <sup>1</sup>H-NMR spectroscopy was carried out to establish the successful incorporation of linker molecules and to detect possible any linker modification. Ce-CAU-24 was dissolved in a mixture of 10 % deuteriochloric acid (DCl) in D<sub>2</sub>O and deuterated dimethyl sulfoxide (d<sub>6</sub>-DMSO) (molar ratio 1:7) before <sup>1</sup>H-NMR spectra were recorded. Zr-CAU-24 was dissolved in a mixture of 50 % deuteriosulfuric acid (D<sub>2</sub>SO<sub>4</sub>) in D<sub>2</sub>O and deuterated dimethyl sulfoxide (d<sub>6</sub>-DMSO) (molar ratio 1:7) before <sup>1</sup>H-NMR spectra were recorded.

**Synthesis of Zr-CAU-24.** All products were synthesized using Pyrex glass reaction tubes (maximum volume 8 mL). 1,2,4,5-Tetrakis(4-carboxyphenyl)benzene (H<sub>4</sub>TCPB, 29.8 mg, 53.3 μmol) was introduced into the glass reactor. After the addition of N,N-dimethylformamide (DMF; 1.5 mL) and formic acid (99%, HCOOH, 1030 μL, 27.3 mmol) an aqueous solution of zirconium(IV) dinitrate oxide hydrate (500 μL, 0.5333 M) was added. The glass reactor was sealed and heated using an aluminum heater block under stirring for 15 min at 100 °C. The colorless precipitate was centrifuged in the mother liquor, which was then decanted off, before being re-dispersed and centrifuged twice in DMF (2 mL). To remove DMF from the product, the solid was washed and centrifuged with acetone (2 mL) four times. The resulting white solid was dried in air at 70 °C.

**Synthesis of Ce-CAU-24.** All products were synthesized using Pyrex glass reaction tubes (maximum volume 8 mL). 1,2,4,5-Tetrakis(4-carboxyphenyl)benzene (H<sub>4</sub>TCPB, 29.8 mg, 53.3 μmol) was introduced into the glass reactor. After the addition of N,N-dimethylformamide (DMF; 1.2 mL) and formic acid (99%, HCOOH, 258 μL, 6.83 mmol) an aqueous solution of cerium(IV) ammonium nitrate (400 μL, 1.066 M) was added. The glass reactor was sealed and heated using an aluminum heater block under stirring for 15 min at 100 °C. The yellow precipitate was centrifuged in the mother liquor, which was then decanted off, before being re-dispersed and centrifuged twice in DMF (2 mL). To remove DMF from the product, the solid was washed and centrifuged with acetone (2 mL) four times. The resulting white solid was dried in air at 70 °C.

Tab. S1. Summary of the most reported Zr-MOFs with tetradeятate linker molecules.

Linker molecule	Compound	Thermal stability	Reference
	MOF-812 [Zr <sub>6</sub> O <sub>4</sub> (OH) <sub>4</sub> (MTB) <sub>3</sub> (H <sub>2</sub> O) <sub>2</sub> ]	-	H. Furukawa, F. G��ndara, Y.-B. Zhang, J. Jiang, W. L. Queen, M. R. Hudson and O. M. Yaghi, <i>J. Am. Chem. Soc.</i> , <b>2014</b> , <i>136</i> , 4369-4381.
<b>MTB<sup>4-</sup></b>			
	MOF-841 [Zr <sub>6</sub> O <sub>4</sub> (OH) <sub>4</sub> (MTB) <sub>2</sub> (HCOO) <sub>4</sub> (H <sub>2</sub> O) <sub>2</sub> ]	~400 °C (TG, air flow)	H. Furukawa, F. G��ndara, Y.-B. Zhang, J. Jiang, W. L. Queen, M. R. Hudson and O. M. Yaghi, <i>J. Am. Chem. Soc.</i> , <b>2014</b> , <i>136</i> , 4369-4381.
<b>MTB<sup>4-</sup></b>			
	Zr-TCPS [Zr <sub>6</sub> O <sub>4</sub> (OH) <sub>4</sub> (TCPS) <sub>2</sub> (H <sub>2</sub> O) <sub>4</sub> (OH) <sub>4</sub> ]	250 °C (XRD)	S. Wang, J. Wang, W. Cheng, X. Yang, Z. Zhang, Y. Xu, H. Liu, Y. Wu, M. Fang, <i>Dalton Trans.</i> <b>2015</b> , <i>44</i> , 8049-8061.
<b>TCPS<sup>4-</sup></b>			
	PCN-94 [Zr <sub>6</sub> O <sub>4</sub> (OH) <sub>4</sub> (ETTC) <sub>3</sub> ]	~ 430 °C (TG, N <sub>2</sub> flow)	Z. Wei, Z.-Y. Gu, R. K. Arvapally, Y.-P. Chen, R. N. McDougald, J. F. Ivy, A. A. Yakovenko, D. Feng, M. A. Omary, H.-C. Zhou, <i>J. Am. Chem. Soc.</i> <b>2014</b> , <i>136</i> , 8269-8276.
<b>ETTC<sup>4-</sup></b>			
	NU-1000 [Zr <sub>6</sub> (μ <sub>3</sub> -OH) <sub>8</sub> (OH) <sub>8</sub> (TBAPy) <sub>2</sub> ]	500 °C (TG, N <sub>2</sub> flow)	J. E. Mondloch, W. Bury, D. Fairén-Jimenez, S. Kwon, E. J. DeMarco, M. H. Weston, A. A. Sarjeant, S. T. Nguyen, P. C. Stair, R. Q. Snurr, O. K. Farha, J. T. Hupp, <i>J. Am. Chem. Soc.</i> <b>2013</b> , <i>135</i> , 10294-10297.
<b>TBAPy<sup>4-</sup></b>			
	Zr-BTBA [Zr <sub>6</sub> O <sub>4</sub> (OH) <sub>4</sub> (BTBA) <sub>3</sub> ]	~ 410 °C (TG, air flow)	S. B. Kalidindi, S. Nayak, M. E. Briggs, S. Jansat, A. P. Katsoulidis, G. J. Miller, J. E. Warren, D. Antypov, F. Cor��, B. Slater, M. R. Prestly, C. Mart��-Gastaldo, M. J. Rosseinsky, <i>Angew. Chem. Int. Ed.</i> <b>2015</b> , <i>54</i> , 221-226.
<b>BTBA<sup>4-</sup></b>			

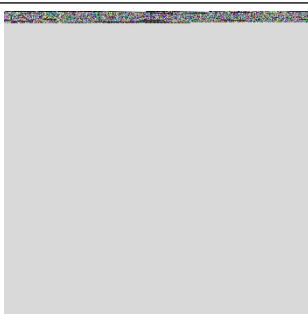
	Zr-PTBA [Zr6O4(OH)4(PTBA)3]	~410 °C (TG, air flow)	S. B. Kalidindi, S. Nayak, M. E. Briggs, S. Jansat, A. P. Katsoulidis, G. J. Miller, J. E. Warren, D. Antypov, F. Corà, B. Slater, M. R. Prestly, C. Martí-Gastaldo, M. J. Rosseinsky, <i>Angew. Chem. Int. Ed.</i> <b>2015</b> , <i>54</i> , 221-226.
	NU-1100 [Zr6O4(OH)4(PTBA)3]	500 °C (TG, N2 flow)	O. V. Gutov, W. Bury, D. A. Gomez-Gualdrón, V. Krungleviciute, D. Fairen-Jimenez, J. E. Mondloch, A. A. Sarjeant, S. S. Al-Juaid, R. Q. Snurr, T. Hupp, T. Yildirim, O. K. Farha, <i>Chem. Eur. J.</i> <b>2014</b> , <i>20</i> , 12389-12393.
	NU-1101 [Zr6O4(OH)4(Py-XP)3]	470 °C (TG, N2 flow)	T. C. Wang, W. Bury, D. A. Gómez-Gualdrón, N. A. Vermeulen, J. E. Mondloch, P. Deria, K. Zhang, P. Z. Moghadam, A. A. Sarjeant, R. Q. Snurr, J. F. Stoddart, J. T. Hupp, O. K. Farha, <i>J. Am. Chem. Soc.</i> <b>2015</b> , <i>137</i> , 3585-3591.
	NU-1102 [Zr6O4(OH)4(Py-PTP)3]	470 °C (TG, N2 flow)	T. C. Wang, W. Bury, D. A. Gómez-Gualdrón, N. A. Vermeulen, J. E. Mondloch, P. Deria, K. Zhang, P. Z. Moghadam, A. A. Sarjeant, R. Q. Snurr, J. F. Stoddart, J. T. Hupp, O. K. Farha, <i>J. Am. Chem. Soc.</i> <b>2015</b> , <i>137</i> , 3585-3591.
	NU-1103 [Zr6O4(OH)4(Por-PP)3]	470 °C (TG, N2 flow)	T. C. Wang, W. Bury, D. A. Gómez-Gualdrón, N. A. Vermeulen, J. E. Mondloch, P. Deria, K. Zhang, P. Z. Moghadam, A. A. Sarjeant, R. Q. Snurr, J. F. Stoddart, J. T. Hupp, O. K. Farha, <i>J. Am. Chem. Soc.</i> <b>2015</b> , <i>137</i> , 3585-3591.
	NU-1104 [Zr6O4(OH)4(Por-PTP)3]	470 °C (TG, N2 flow)	T. C. Wang, W. Bury, D. A. Gómez-Gualdrón, N. A. Vermeulen, J. E. Mondloch, P. Deria, K. Zhang, P. Z. Moghadam, A. A. Sarjeant, R. Q. Snurr, J. F. Stoddart, J. T. Hupp, O. K. Farha, <i>J. Am. Chem. Soc.</i> <b>2015</b> , <i>137</i> , 3585-3591.

 <b>TCPP<sup>4-</sup></b>	<b>MOF-525</b> $[\text{Zr}_6\text{O}_4(\text{OH})_4(\text{TCPP})_3]$	W. Morris, B. Voloskiy, S. Demir, F. Gándara, P. L. McGrer, H. Furukawa, D. Cascio, J. F. Stoddart, O. M. Yaghi, <i>Inorg. Chem.</i> <b>2012</b> , 51, 6443-6445.
 <b>TCPP<sup>4-</sup></b>	<b>MOF-545</b> $[\text{Zr}_6\text{O}_8(\text{H}_2\text{O})_8(\text{TCPP})_2]$	W. Morris, B. Voloskiy, S. Demir, F. Gándara, P. L. McGrer, H. Furukawa, D. Cascio, J. F. Stoddart, O. M. Yaghi, <i>Inorg. Chem.</i> <b>2012</b> , 51, 6443-6445.
 <b>TCPP<sup>4-</sup></b>	<b>MOF-535</b> $[\text{Zr}_6\text{O}_4(\text{OH})_4(\text{XF})_3]$	W. Morris, B. Voloskiy, S. Demir, F. Gándara, P. L. McGrer, H. Furukawa, D. Cascio, J. F. Stoddart, O. M. Yaghi, <i>Inorg. Chem.</i> <b>2012</b> , 51, 6443-6445.
 <b>TCPP<sup>4-</sup></b>	<b>PCN-221</b>	No M: 360 °C (TG, N <sub>2</sub> flow) D. Feng, H.-L. Jiang, Y.-P. Chen, Z.-Y. Gu, Z. Wei, H.-C. Zhou, <i>Inorg. Chem.</i> <b>2013</b> , 52, 12661-12667.
 <b>TCPP<sup>4-</sup></b>	<b>PCN-222</b> $[\text{Zr}_6(\text{OH})_8(\text{TCPP})_2(\text{OH})_8]$	No M: 350 °C (TG, N <sub>2</sub> flow) D. Feng, Z.-Y. Gu, J.-R. Li, H.-L. Jiang, Z. Wei, H.-C. Zhou, <i>Angew. Chem. Int. Ed.</i> <b>2012</b> , 51, 10307-10310.



PCN-223  
[Zr<sub>6</sub>O<sub>4</sub>(OH)<sub>4</sub>(TCPP)<sub>3</sub>]

~ 350 °C (TG, N<sub>2</sub> flow) D. Feng, Z.-Y. Gu, Y.-P. Chen, J. Park, Z. Wei, Y. Sun, M. Bosch, S. Yuan, H.-C. Zhou, *J. Am. Chem. Soc.* **2014**, *136*, 17714-17717.



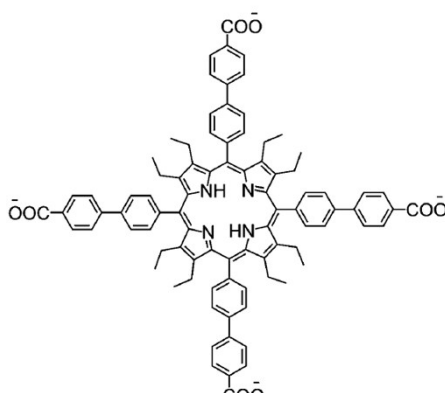
PCN-224  
[Zr<sub>6</sub>O<sub>4</sub>(OH)<sub>4</sub>(TCPP)<sub>1.5</sub>(OH)<sub>6</sub>(H<sub>2</sub>O)<sub>6</sub>]

No M: 350 °C (TG, N<sub>2</sub> flow) D. Feng, W.-C. Chung, Z. Wei, Z.-Y. Gu, H.-L. Jiang, Y.-P. Chen, D. J. Daresbourg, H.-C. Zhou, *J. Am. Chem. Soc.* **2013**, *135*, 17105-17110.



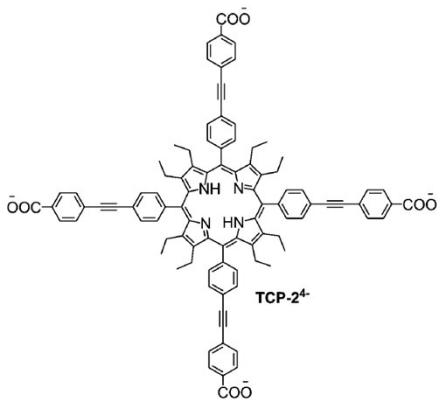
PCN-225  
[Zr<sub>6</sub>O<sub>4</sub>(OH)<sub>4</sub>(TCPP)<sub>2</sub>(OH)<sub>4</sub>(H<sub>2</sub>O)<sub>4</sub>]

470 °C (TG, N<sub>2</sub> flow) H.-L. Jiang, D. Feng, K. Wang, Z.-Y. Gu, Z. Wei, Y.-P. Chen, H.-C. Zhou, *J. Am. Chem. Soc.* **2013**, *135*, 13934-13938.

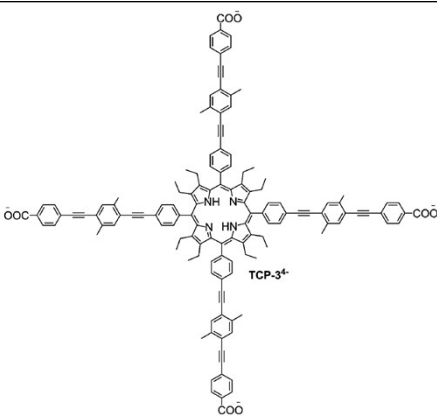


PCN-228  
[Zr<sub>6</sub>O<sub>4</sub>(OH)<sub>4</sub>(TCP-1)<sub>3</sub>]

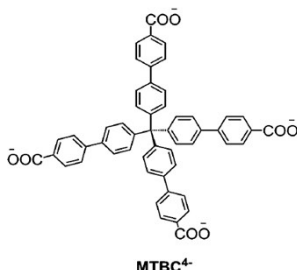
T.-F. Liu, D. Feng, Y.-P. Chen, L. Zou, M. Bosch, S. Yuan, Z. Wei, S. Fordham, K. Wang, H.-C. Zhou, *J. Am. Chem. Soc.* **2015**, *137*, 413-419.



T.-F. Liu, D. Feng, Y.-P. Chen, L. Zou,  
M. Bosch, S. Yuan, Z. Wei, S.  
Fordham, K. Wang, H.-C. Zhou, *J. Am.  
Chem. Soc.* **2015**, *137*, 413-419.



T.-F. Liu, D. Feng, Y.-P. Chen, L. Zou,  
M. Bosch, S. Yuan, Z. Wei, S.  
Fordham, K. Wang, H.-C. Zhou, *J. Am.  
Chem. Soc.* **2015**, *137*, 413-419.



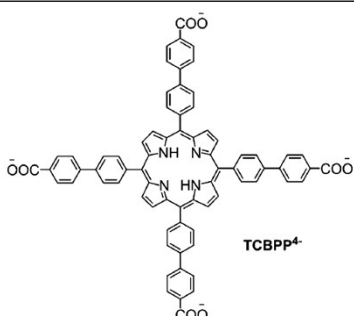
500 °C  
(TG, N<sub>2</sub>  
flow)

M. Zhang, Y.-P. Chen, M. Bosch, T.  
Gentle, K. Wang, D. Feng, Z. U. Wang,  
H.-C. Zhou, *Angew Chem. Int. Ed.*  
**2014**, *53*, 815-818.



**MMFP-6**  
[Zr<sub>6</sub>O<sub>8</sub>(TCPP)<sub>2</sub>(H<sub>2</sub>O)<sub>8</sub>]

Y. Chen, T. Hoang, S. Ma, *Inorg.  
Chem.* **2012**, *51*, 12600-12602.



~ 450 °C  
(TG, N<sub>2</sub>  
flow)

Q. Lin, X. Bu, A. Kong, C. Mao, X.  
Zhao, F. Bu, P. Feng, *J. Am. Chem.  
Soc.* **2015**, *137*, 2235-2238.

## 2. Powder X-ray diffraction

A structural model was developed starting from crystal structures of Zr-MOFs that have already been reported.<sup>[3]</sup> Comparison of the PXRD patterns with the one of PCN-223<sup>[4]</sup> indicated several similarities, however, Rietveld refinement using this topology was unsuccessful. Indexing of the PXRD data of activated Zr-CAU-24 suggested hexagonal as well as C-centered orthorhombic space groups. Assuming the inorganic building unit to be the hexanuclear cluster most frequently observed in Zr-MOFs, a structure model starting from the cubic MOF-525<sup>[5]</sup> was set up. The first step was reducing the symmetry employing a supergroup-subgroup relationship from  $Pm\text{-}3m \rightarrow P4/mmm \rightarrow Cmmm$  (No. 65) using PowderCell<sup>[6]</sup> and adjusting the original lattice parameters to the ones obtained by indexing. Force field calculations were performed to optimize the position of the hexanuclear  $[\text{Zr}_6\text{O}_4(\text{OH})_4]^{12+}$  clusters arranged at the cell edges and C-faces using Material Studio 4.3.<sup>[7]</sup> Replacing the porphyrin linker by TCPB<sup>4+</sup> and removing the linker molecules parallel to the a-c plain yielded a reasonable structure model.

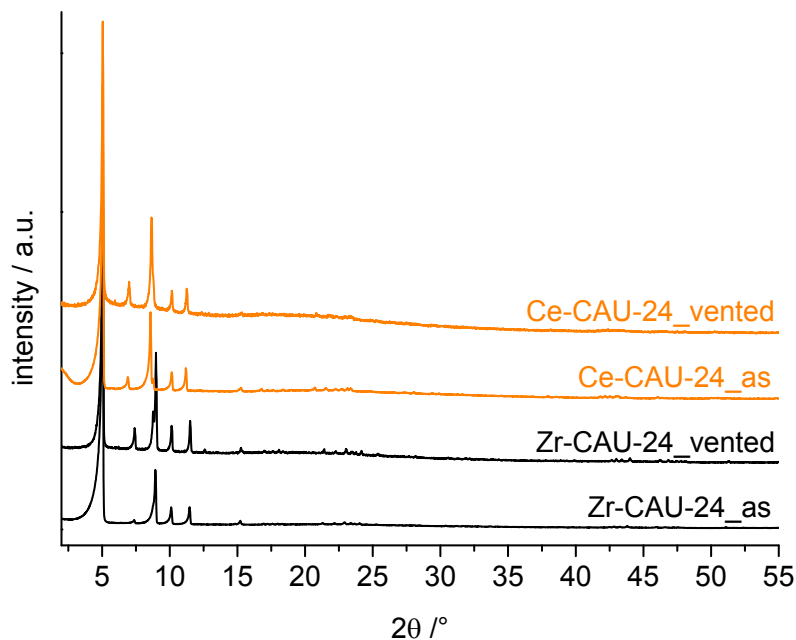


Fig. S1. Comparison of the PXRD pattern ( $\lambda = 1.5406 \text{ \AA}$ ) of as synthesized and thermally treated Zr-CAU-24 and Ce-CAU-24 after storage under ambient conditions for 12 h (vented).

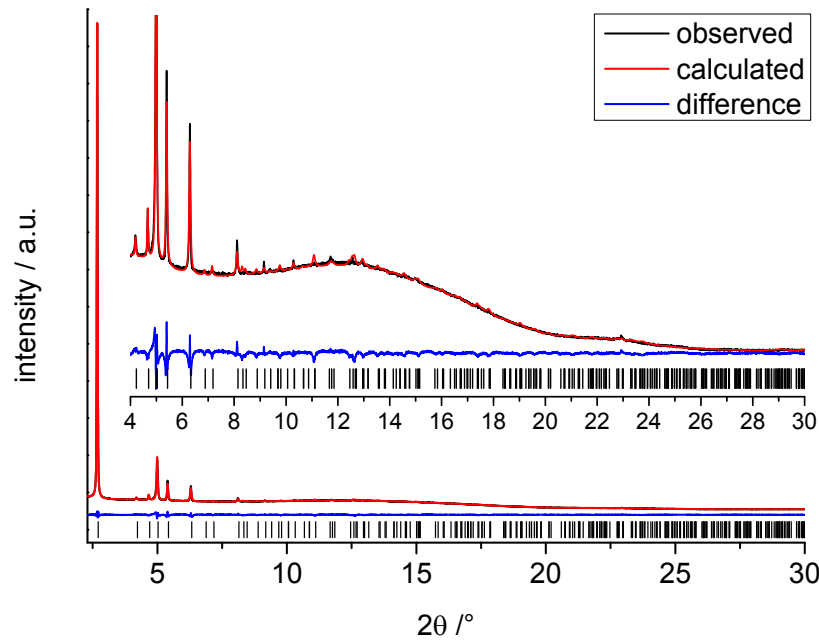


Fig. S2. Final Rietveld plot of Zr-CAU-24\_act. The observed PXRD pattern ( $\lambda = 0.826215 \text{ \AA}$ ) is shown in black, the calculated in red and the difference (observed - calculated) of both patterns is given in blue. The allowed positions of the Bragg peaks are given by as black ticks.

Tab. S2. Crystallographic parameters of activated Zr-CAU-24.

<b>Compound</b>	<b>Zr-CAU-24_act</b>
Formula	[Zr <sub>6</sub> (μ <sub>3</sub> -O) <sub>4</sub> (μ <sub>3</sub> -OH) <sub>4</sub> (OH) <sub>4</sub> (H <sub>2</sub> O) <sub>4</sub> (TCPB) <sub>2</sub> ]
$\lambda/\text{\AA}$	0.826215
Space group	<i>Cmmm</i>
$a/\text{\AA}$	20.141(2)
$b/\text{\AA}$	34.89(1)
$c/\text{\AA}$	11.1939(7)
$R_{wp}/\%$	1.91
$R_{Bragg}/\%$	0.36
GoF	3.38
No. of atoms	20
No. of restraints	24

Tab. S3. Representation of selected bond lengths of Zr-CAU-24\_act.

<b>Atom 1</b>	<b>Atom 2</b>	<b>Distance / Å</b>	<b>Atom 1</b>	<b>Atom 2</b>	<b>Distance / Å</b>
Zr2	O1	2.240(23)	C8	C9	1.467
Zr2	O6	2.305(39)	C7	C10	1.401
Zr1	O6	2.198(23)	C6	C9	1.402
Zr1	O5	2.161(22)	C5	C6	1.386
Zr1	O4	2.199(27)	C4	C5	1.393
Zr1	O3	2.111(24)	C4	C7	1.405
Zr1	O2	2.182(20)	C3	C19	1.434
O2	C8	1.294(24)	C3	C4	1.469
O1	C8	1.254(22)			

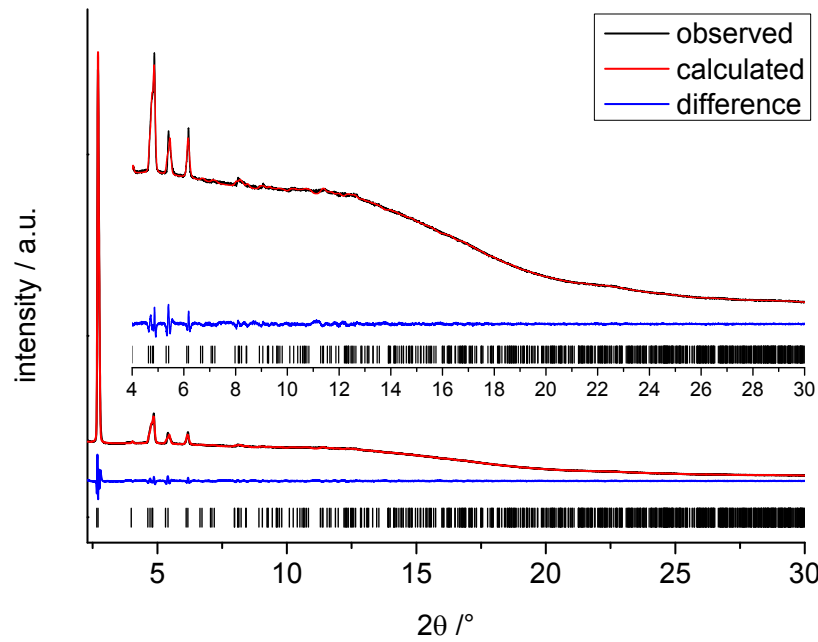


Fig. S3. Le Bail plot of Ce-CAU-24\_act. The observed PXRD pattern ( $\lambda=0.825927\text{ \AA}$ ) is shown in black, the calculated in red and the difference (observed - calculated) of both patterns is given in blue. The allowed positions of the Bragg peaks are given by as black tics.

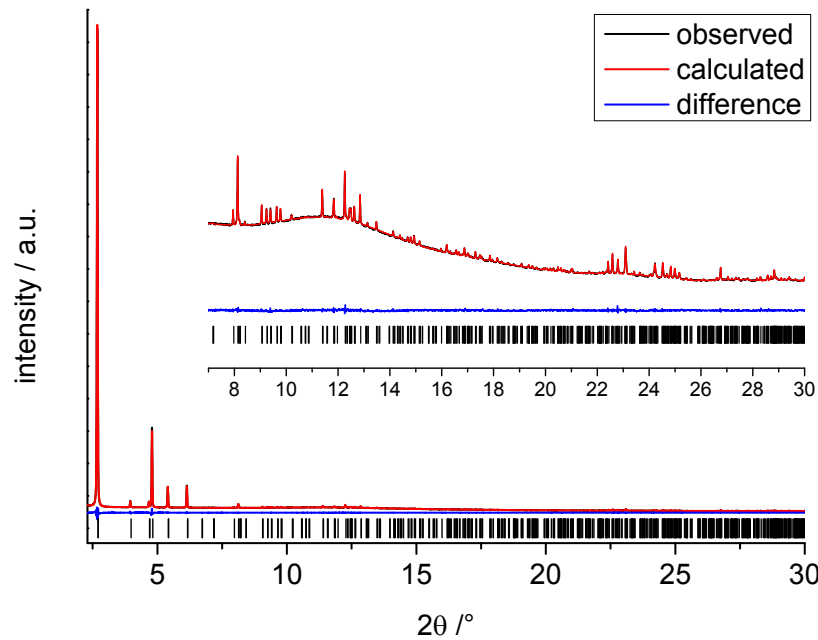


Fig. S4. Le Bail plot of Zr-CAU-24\_as. The observed PXRD pattern ( $\lambda=0.826215\text{ \AA}$ ) is shown in black, the calculated in red and the difference (observed - calculated) of both patterns is given in blue. The allowed positions of the Bragg peaks are given by as black tics.

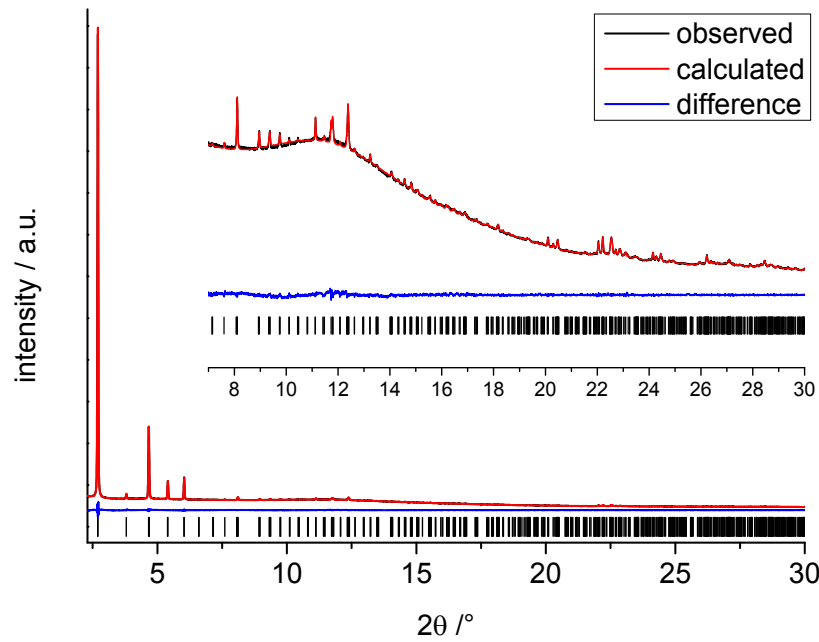


Fig. S5. Le Bail plot of Ce-CAU-24<sub>as</sub>. The observed PXRD pattern ( $\lambda = 0.825927 \text{ \AA}$ ) is shown in black, the calculated in red and the difference (observed - calculated) of both patterns is given in blue. The allowed positions of the Bragg peaks are given by as black tics.

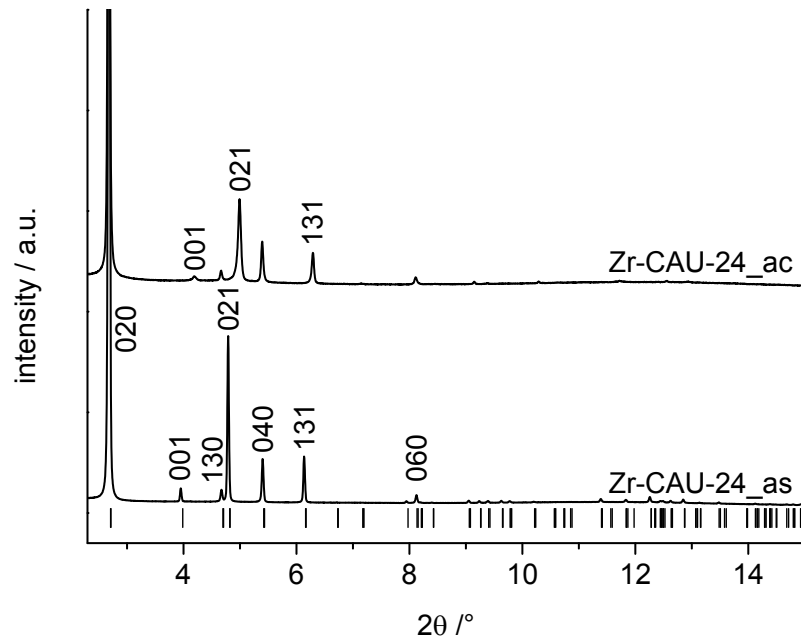


Fig. S6. Shift of the (001)-, (021)-, and (131)-reflections during activation of Zr-CAU-24<sub>as</sub>.

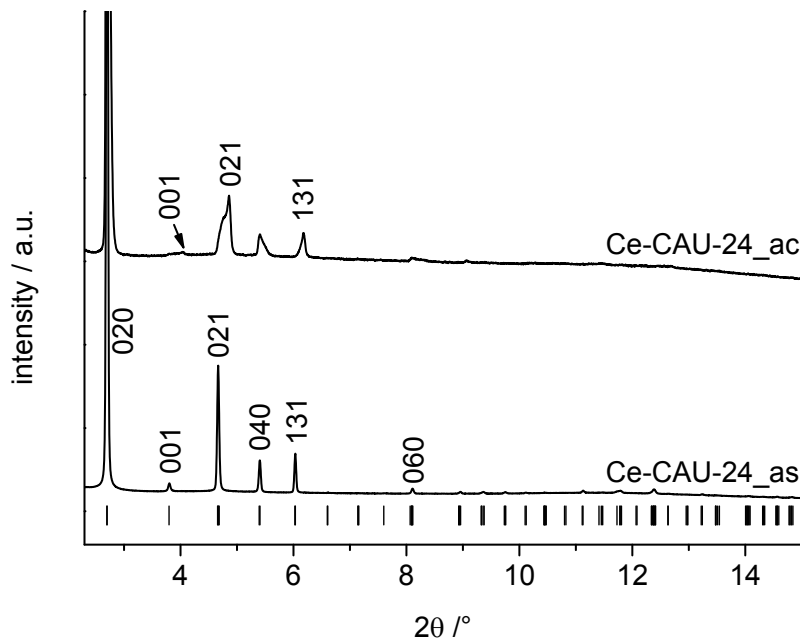
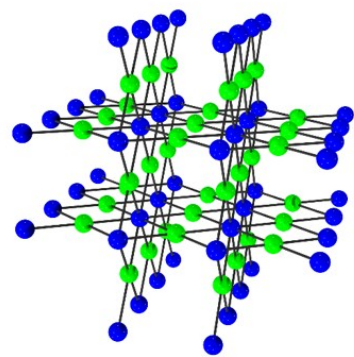


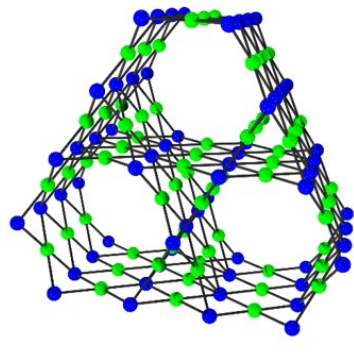
Fig. S7. Shift of the (001)-, (021)-, and (131)-reflections during activation of Ce-CAU-24\_as.

Tab. S4. Crystallographic data of the compounds Zr-CAU-24\_as, Zr-CAU-24\_act, Ce-CAU-24\_as and Ce-CAU-24\_act. Lattice parameters for Zr-CAU-24\_as, Ce-CAU-24\_as and Ce-CAU-24\_act were obtained using the Le Bail method.

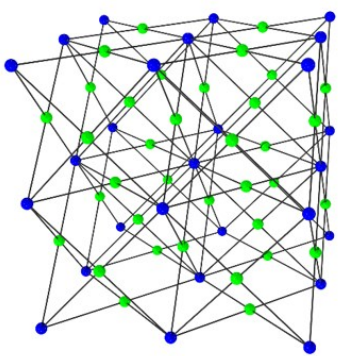
Compound	Zr-CAU-24_		Ce-CAU-24_	
	as	act	as	act
SG	<i>Cmmm</i>	<i>Cmmm</i>	<i>Cmmm</i>	<i>Cmmm</i>
$\lambda [\text{\AA}]$	0.826215	0.826215	0.825927	0.825927
$a [\text{\AA}]$	20.1112(2)	20.141(2)	20.2081(5)	20.099(6)
$b [\text{\AA}]$	34.944(1)	34.89(1)	35.1067(7)	35.19(1)
$c [\text{\AA}]$	11.8792(1)	11.1939(7)	12.4622(1)	11.778(2)
$R_{wp} / \%$	1.85	1.91	1.13	1.61
GoF	3.48	3.38	2.49	3.30



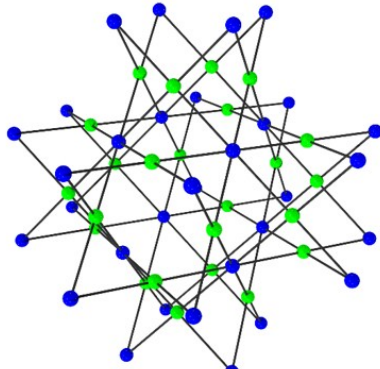
**scu**  
(4,8)-connected



**csq**  
(4,8)-connected



**ftw**  
(4,12)-connected



**she**  
(4,6)-connected

Fig. S8. Representation of prominent topologies of Zr-MOFs with tetradentate linker molecules and the scu topology, which was observed for the first time for Zr-based MOFs in this study.

### 3. Thermal Analysis

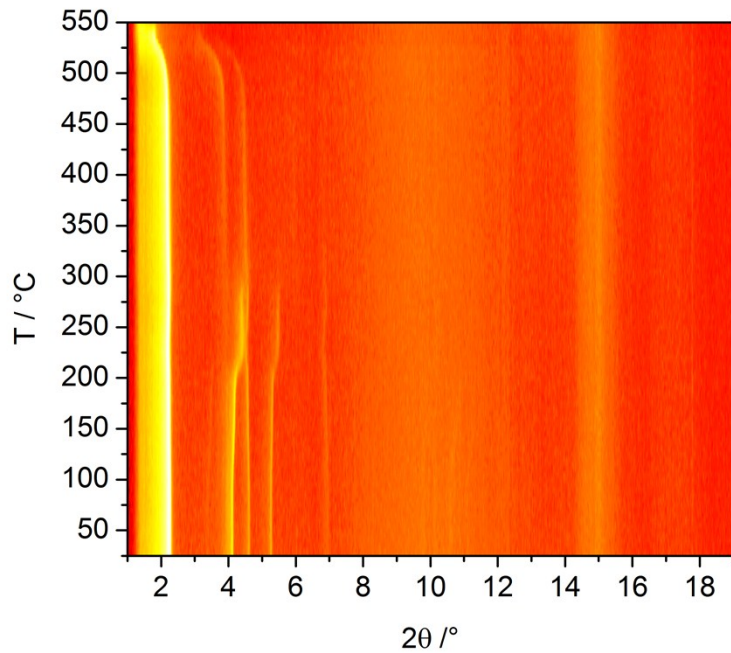


Fig. S9. Results of the temperature dependent PXRD measurement of Zr-CAU-24 in top view.

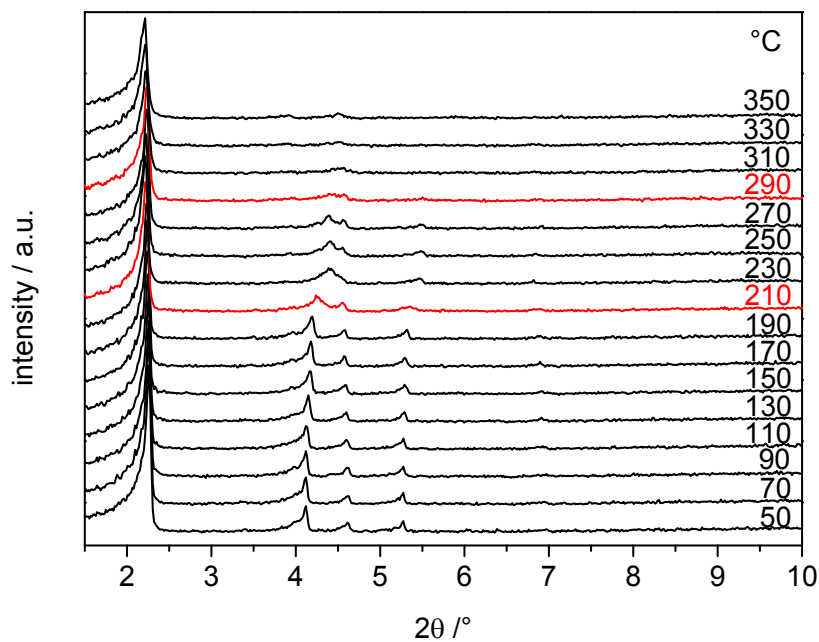


Fig. S10. Temperature dependent PXRD patterns of Zr-CAU-24. Structural changes are marked in red.

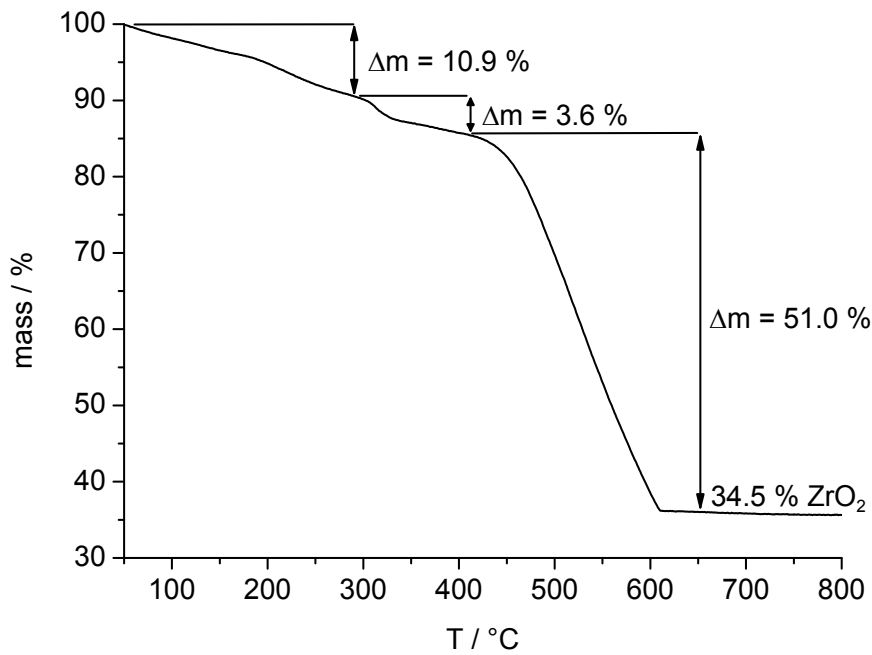


Fig. S11 TG curve of as synthesized Zr-CAU-24 heated under air flow.

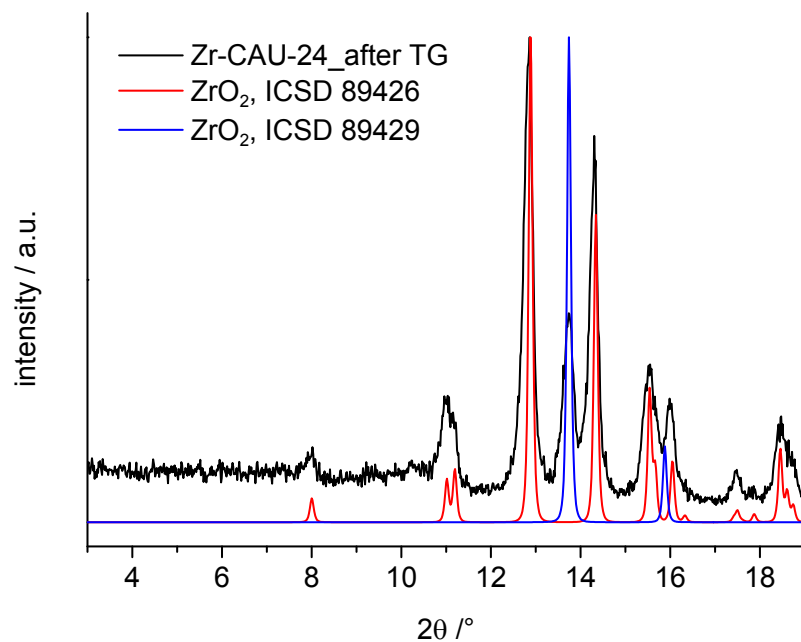


Fig. S12. Comparison of the PXRD pattern of Zr-CAU-24 after thermogravimetric analysis with theoretical PXRD of cubic ZrO<sub>2</sub> (ICSD 89429) and monocline ZrO<sub>2</sub> (Baddelyite, ICSD 89426).

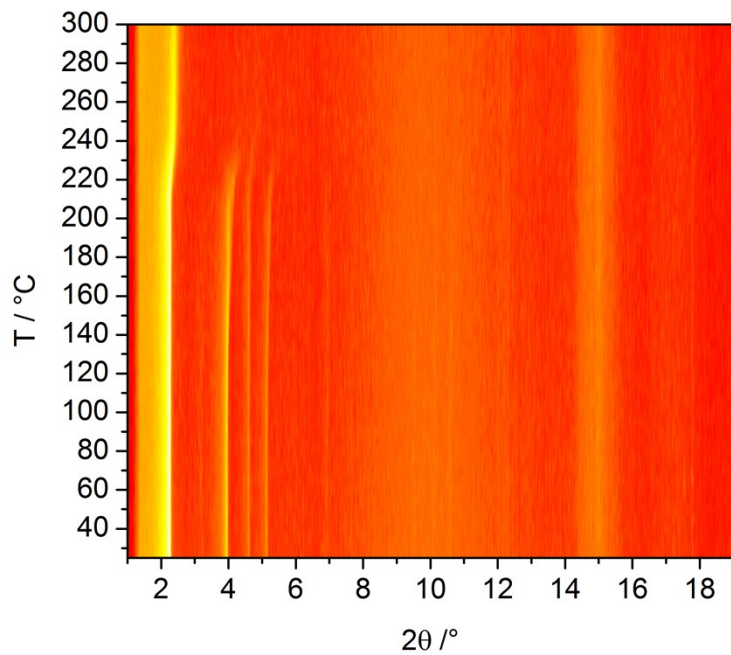


Fig. S13. Results of the temperature dependent PXRD measurement of Ce-CAU-24 in top view.

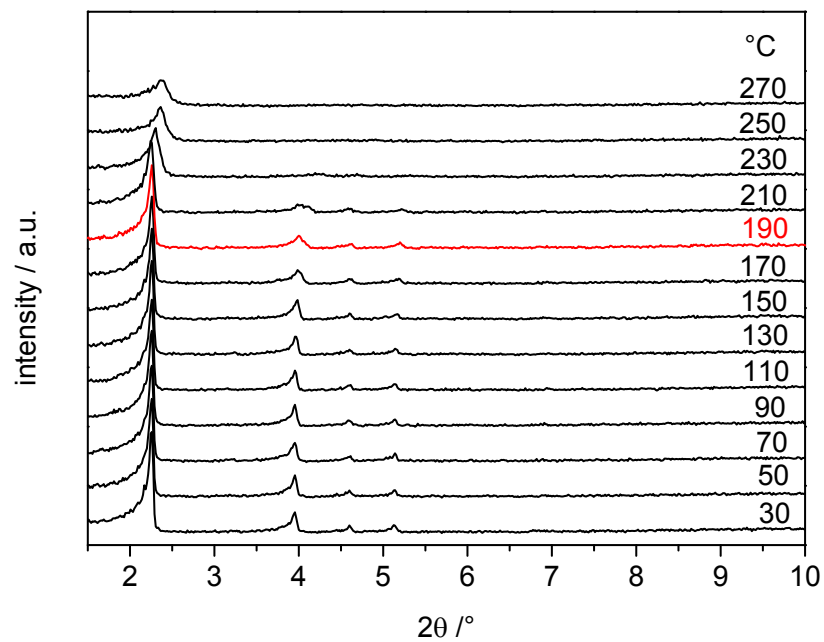


Fig. S14. Temperature dependent PXRD patterns of Ce-CAU-24. Structural change is marked in red.

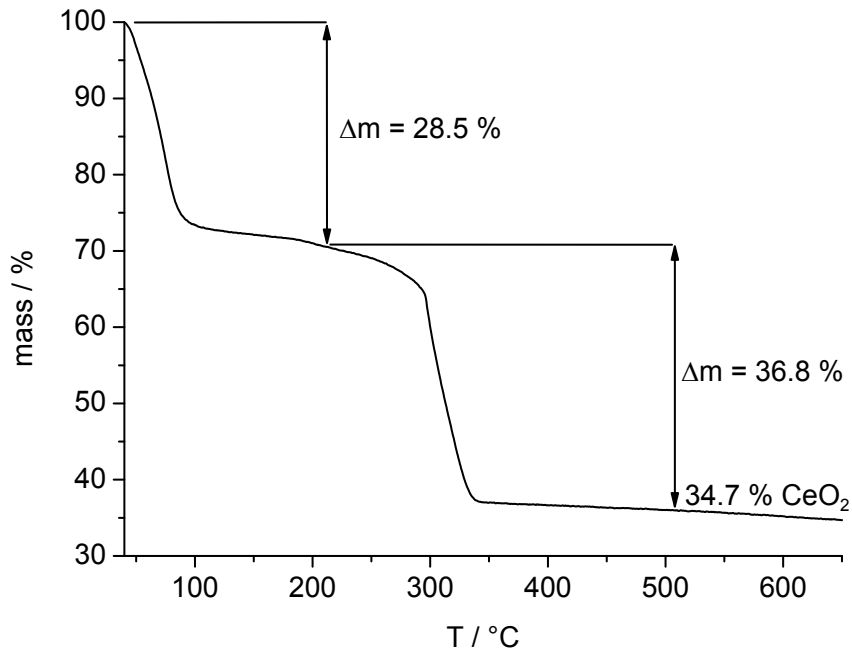


Fig. S15. TG curve of as synthesized Ce-CAU-24 heated under air flow.

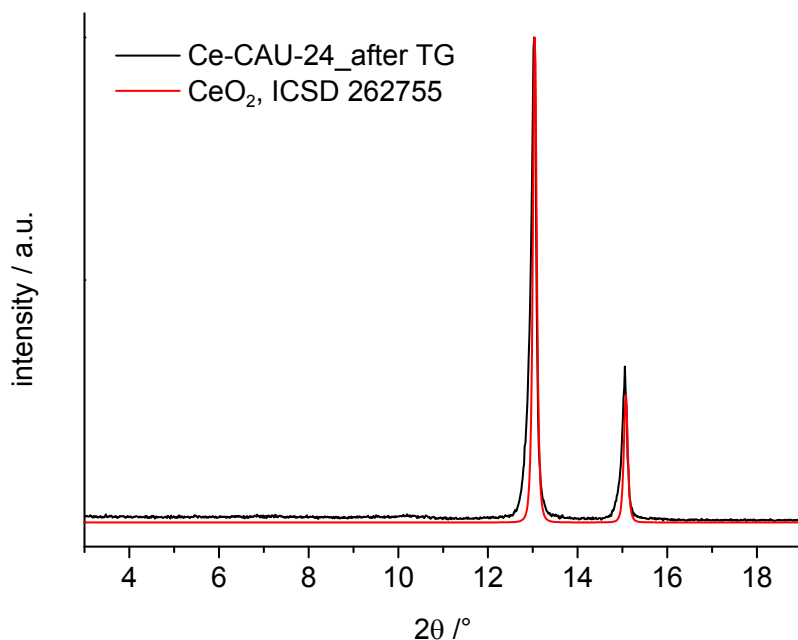


Fig. S16. Comparison of the PXRD pattern of Ce-CAU-24 after thermogravimetric analysis with theoretical PXRD of cubic CeO<sub>2</sub> (ICSD 262755).

#### 4. IR spectroscopy

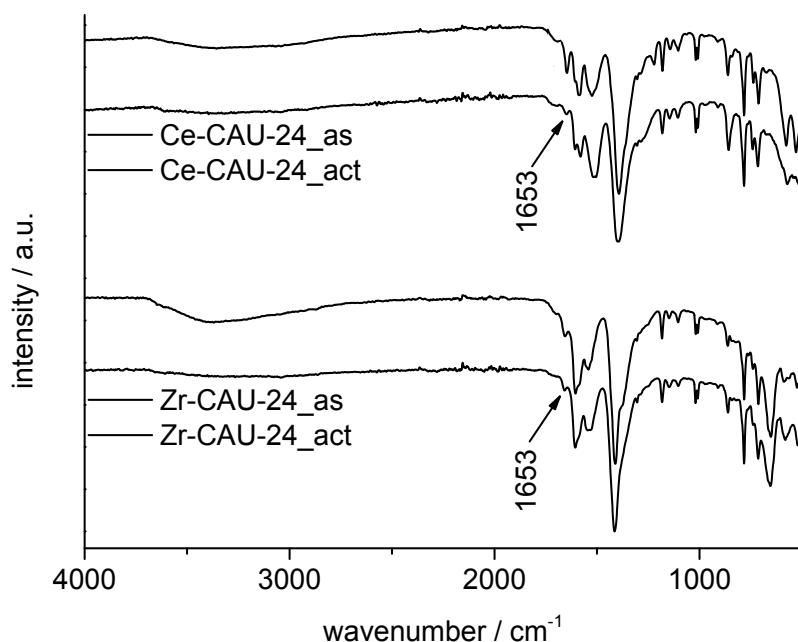


Fig. S17. IR spectra of as synthesized and activated (140 °C and 10<sup>-2</sup> kPa) Zr-CAU-24 and Ce-CAU-24.

Tab. S5. Assignment of the IR vibrations observed for Zr-CAU-24\_as and Ce-CAU-24\_as.<sup>[8]</sup>

Vibration	Intensity	Zr-CAU-24_as wavenumber [cm <sup>-1</sup> ]	Ce-CAU-24_as wavenumber [cm <sup>-1</sup> ]
v (H <sub>2</sub> O)	w	3600-3000	3600-3000
v <sub>as</sub> (C=O) carbonyl group of DMF	w	1653	1653
v <sub>as</sub> (COO <sup>-</sup> ) carbonyl group of formate	m	1606	1606
v <sub>as</sub> (COO <sup>-</sup> ) carbonyl group of TCPB <sup>4-</sup>	m	1588	1581
v (C=C) aromatic rings	m	1544, 1531	1518, 1504
v <sub>s</sub> (COO <sup>-</sup> ) carbonyl group of TCPB <sup>4-</sup>	s	1415	1397
v (C-H) substituted benzene ring	m	860, 782	860, 782
v (Zr-O)	s	650	-
v (Ce-O)	s	-	570

## 5. NMR spectroscopy

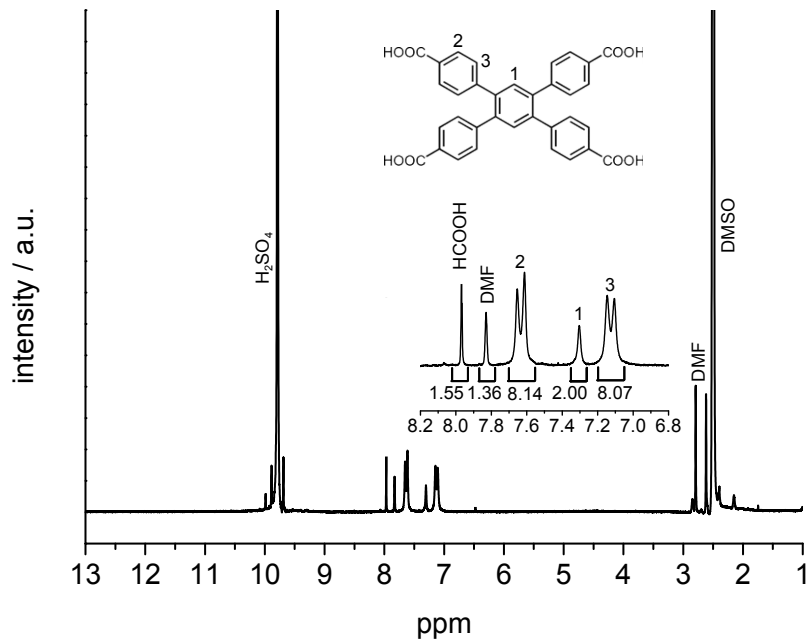


Fig. S18. <sup>1</sup>H-NMR spectrum of dissolved Zr-CAU-24<sub>as</sub>.

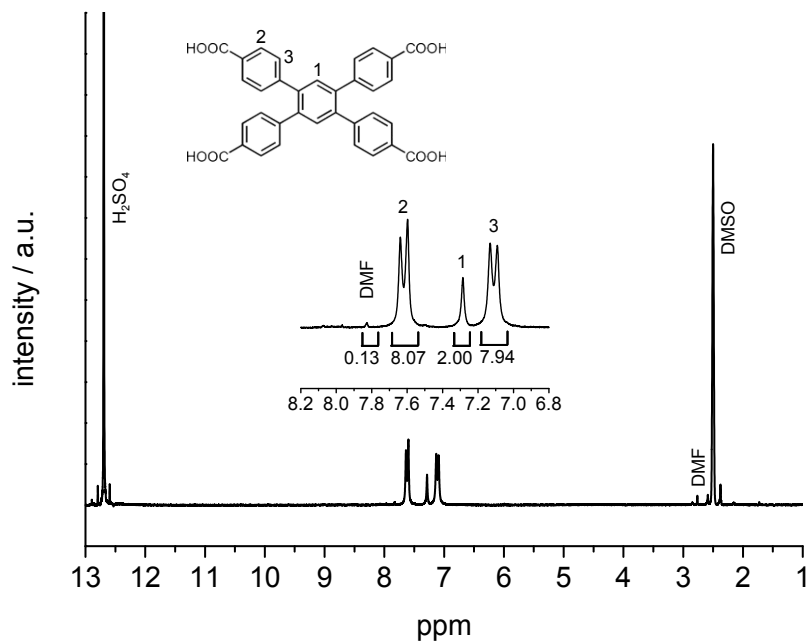


Fig. S19. <sup>1</sup>H-NMR spectrum of activated (140 °C and 10<sup>-2</sup> kPa) and then dissolved Zr-CAU-24.

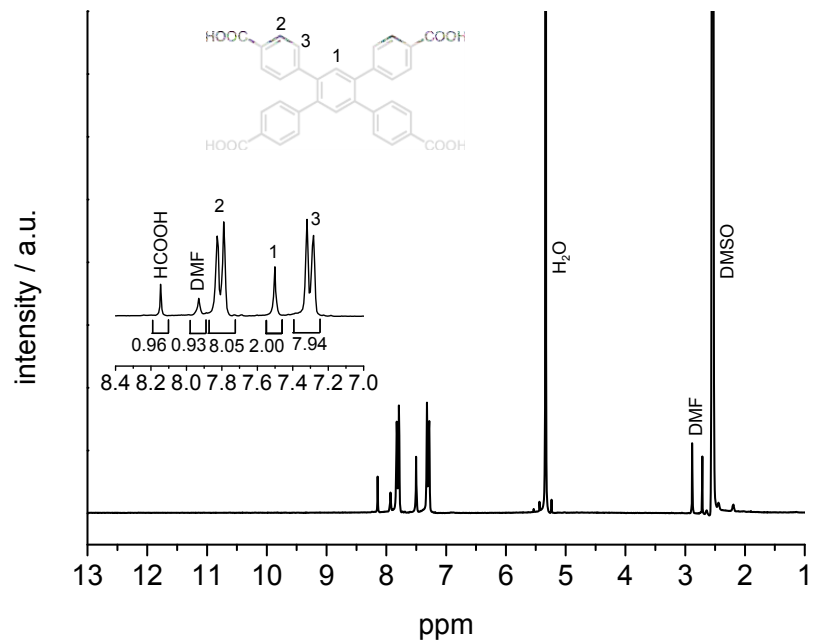


Fig. S20. <sup>1</sup>H-NMR spectrum of dissolved Ce-CAU-24<sub>as</sub>.

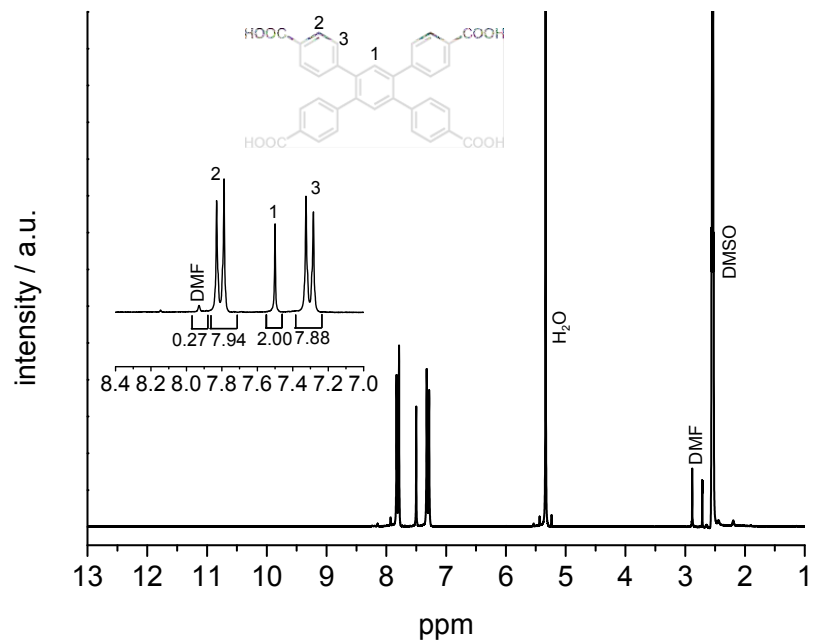


Fig. S21. <sup>1</sup>H-NMR spectrum of activated (140 °C and 10<sup>-2</sup> kPa) and then dissolved Ce-CAU-24.

## 6. N<sub>2</sub> sorption measurements

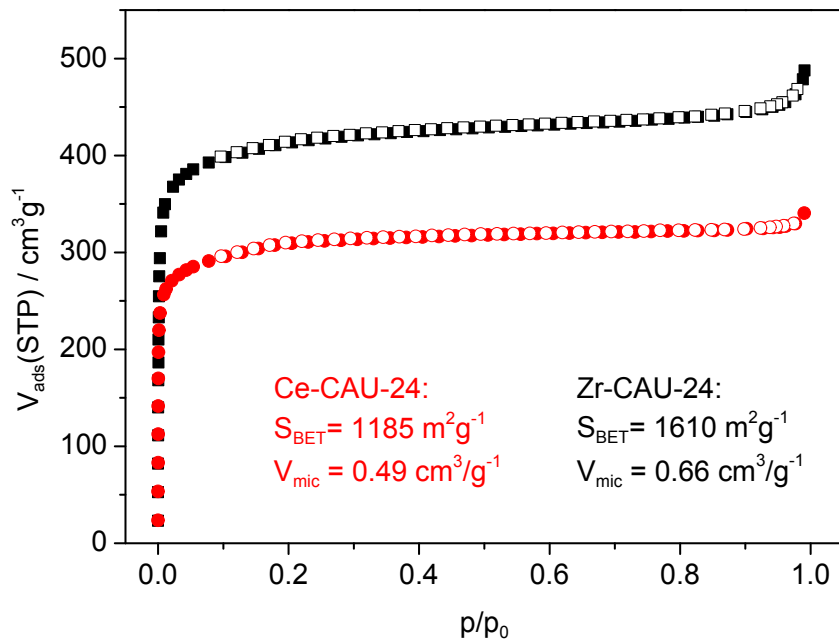


Fig. S22. Results of N<sub>2</sub> sorption measurements of activated (140 °C, 10<sup>-2</sup> kPa) Zr-CAU-24 and Ce-CAU-24. Filled symbols mark the adsorption, while empty symbols mark the desorption step.

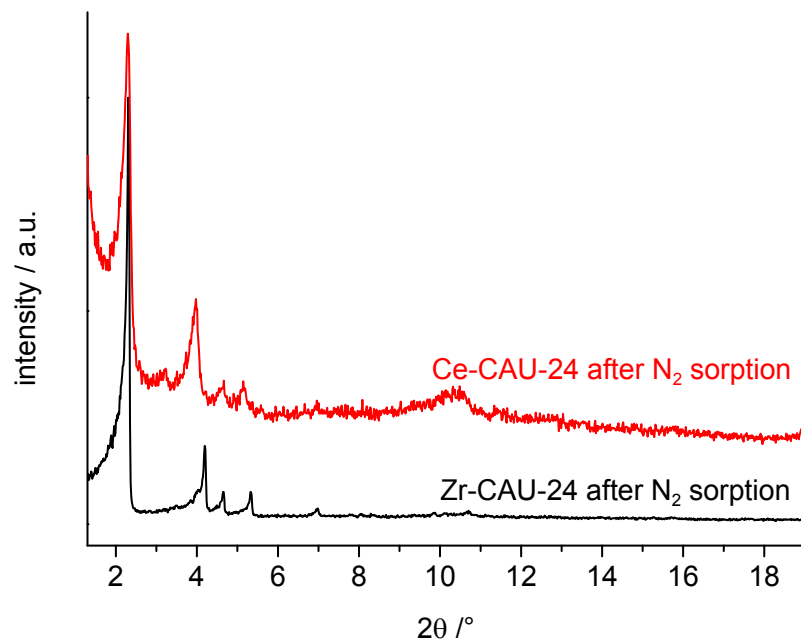


Fig. S23. PXRD patterns of Zr-CAU-24 and Ce-CAU-24 after N<sub>2</sub> sorption measurement.

Tab. S6. Specific surface areas and micropore volumes of Zr-CAU-24 and Ce-CAU-24. For comparison the specific surface are given in  $\text{m}^2\text{g}^{-1}$  and  $\text{m}^2\mu\text{mol}^{-1}$ .

	Zr-CAU-24	Ce-CAU-24
$V_m [\text{cm}^3\text{g}^{-1}]$	0.66	0.49
$S_{\text{BET}} [\text{m}^2\text{g}^{-1}]$	1610	1185
$S_{\text{BET}} [\text{m}^2\mu\text{mol}^{-1}]$	3.10	2.59

## 7. Luminescence measurements

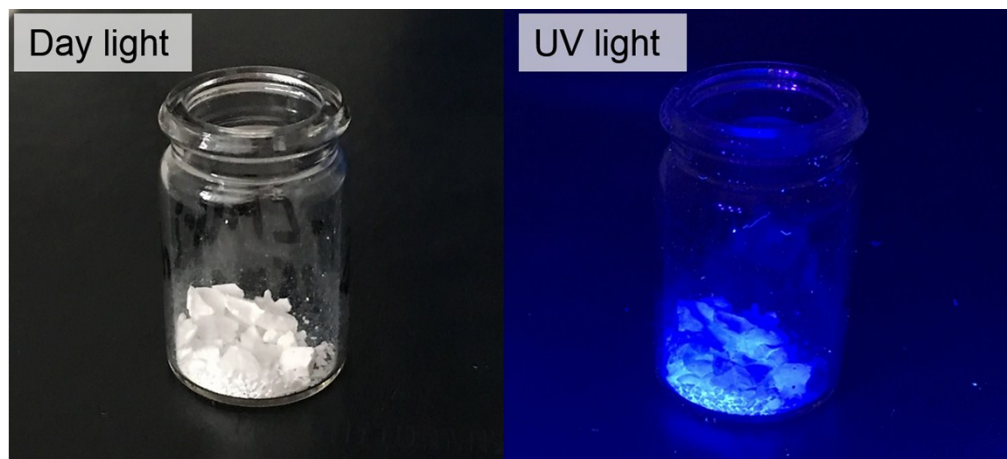


Fig. S24: Zr-CAU-24 sample under day light (left-hand side) and UV radiation ( $27397 \text{ cm}^{-1}$ , right-hand side).

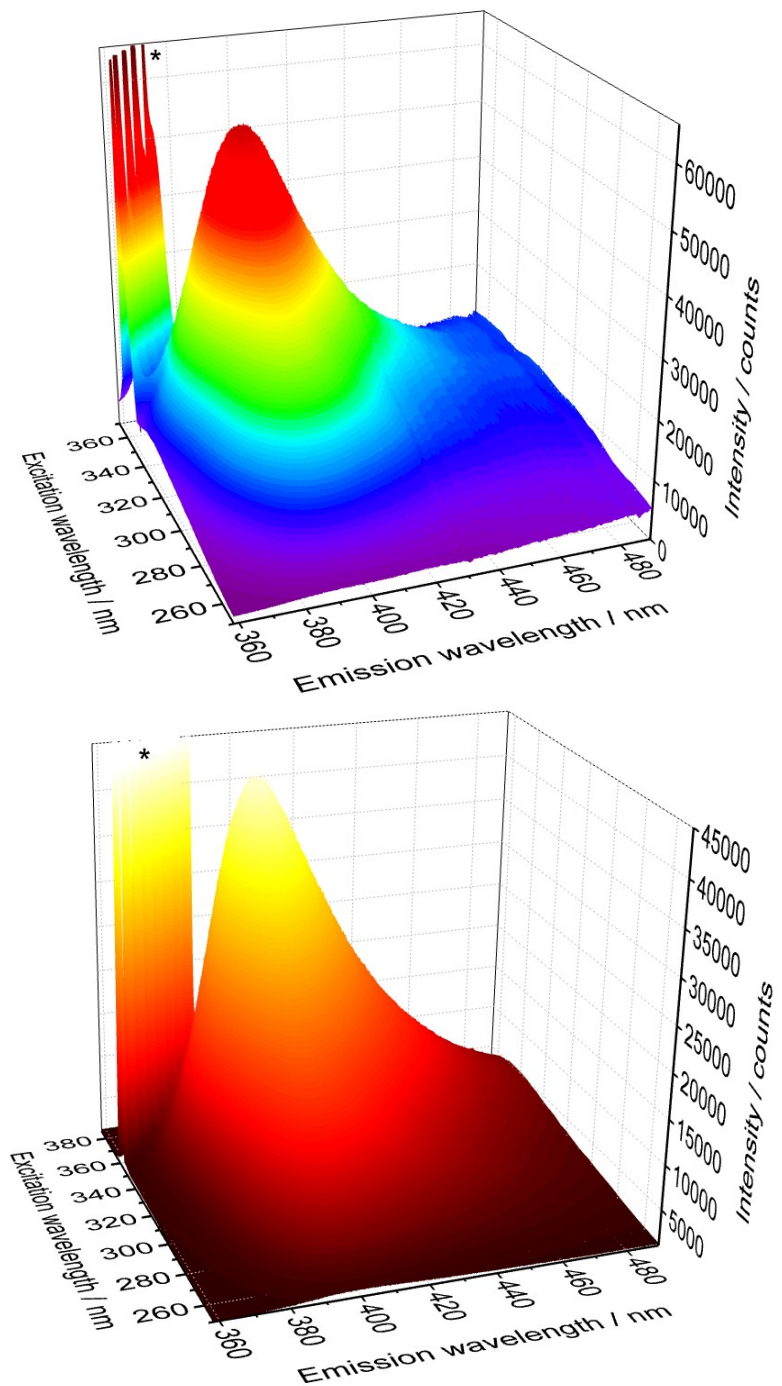


Fig. S25: 3D plot of emission and excitation spectra for Zr-CAU-24 (top) and the  $\text{H}_4\text{TCPB}$  ligand (bottom). The asterisk (\*) signs indicate the peak related to the excitation source.

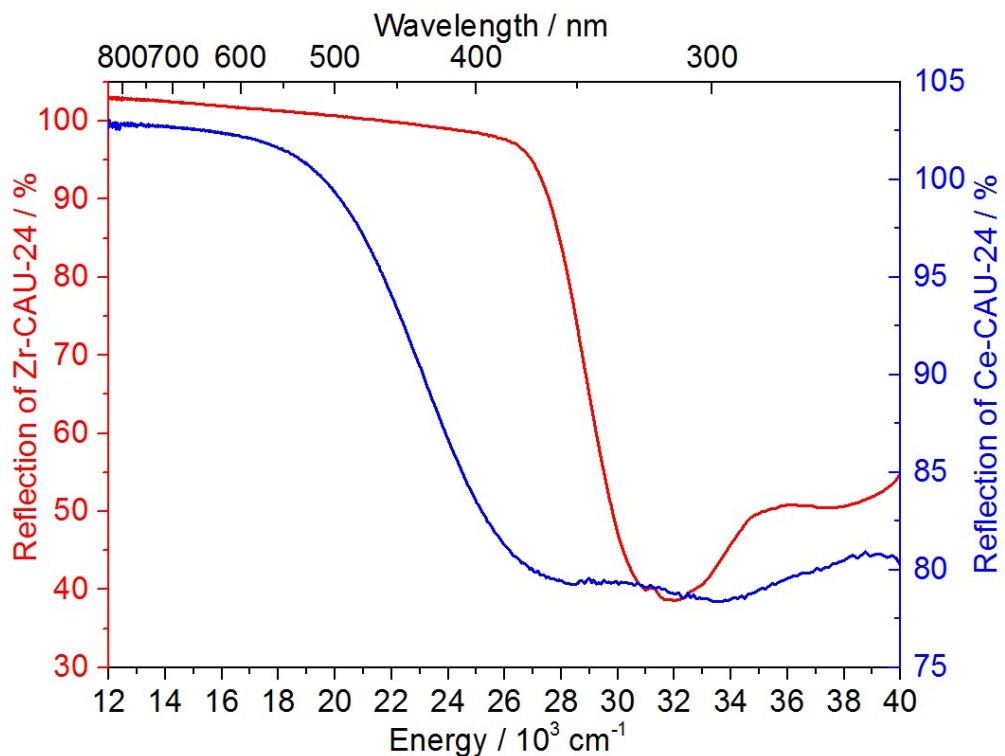


Fig. S26: Reflection spectra of Zr-CAU-24 (red curve) and Ce-CAU-24 (blue curve).

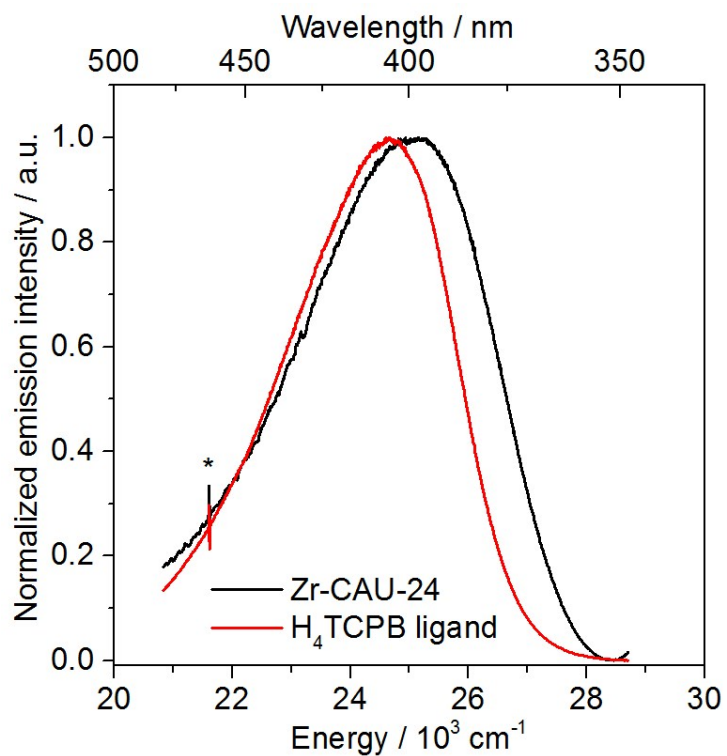


Fig. S27: Emission spectra ( $\tilde{\nu}_{\text{ex}} = 29411 \text{ cm}^{-1}$ ) of Zr-CAU-24 MOF (black curve) and H<sub>4</sub>TCPB ligand (red curve). The asterisk (\*) sign indicates an artefact of the correction of the CCD detector.

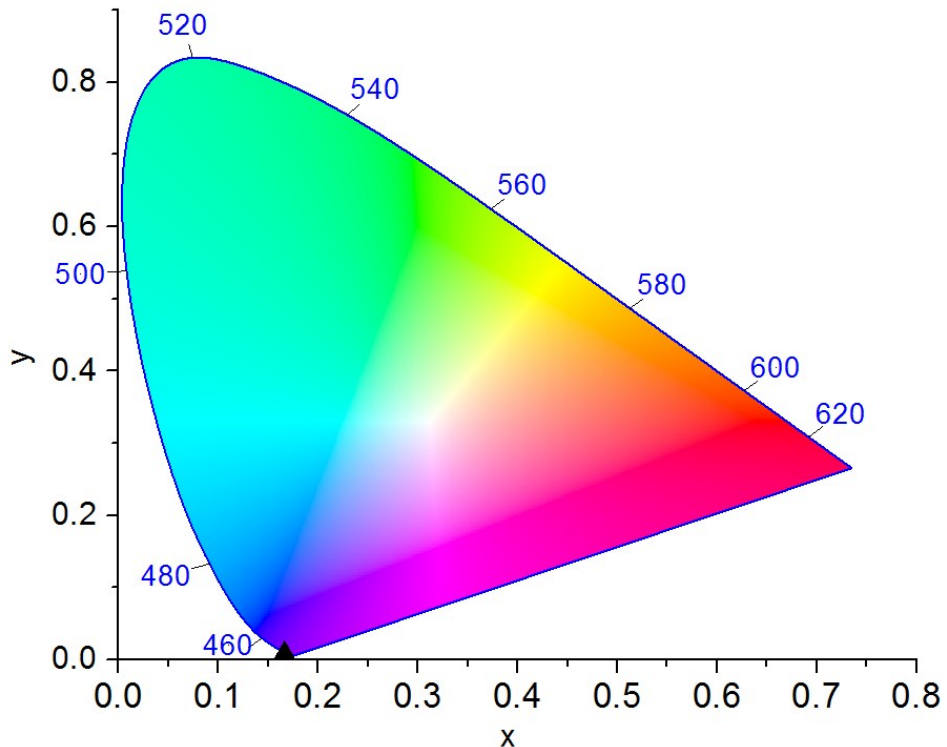


Fig. S28: Plot of colour coordinates  $x = 0.1666$ ,  $y = 0.0105$  ( $\blacktriangle$ ) on the CIE (Commission internationale de l'éclairage) 1931<sup>[9-11]</sup> chromaticity diagram for Zr-CAU-24, calculated from the respective measured emission spectrum (Fig. S28) applying the Spectra Lux Software v.2.0.<sup>[1]</sup>

- 
- 1 P.A. Santa-Cruz, F.S. Teles, SpectraLux Software v. 2.0, Ponto Quântico Nano-dispositivos/RENAMI, Recife-PE Brazil, 2003.
  - 2 S.P. Thompson, J.E. Parker, J. Marchal, J. Potter, A. Birt, F. Yuan, R.D. Fearn, A.R. Lennie, S.R. Street and C.C. Tang, *J. Synchrotron Radiat.*, 2011, **18**, 637-648.
  - 3 S. Huh, S.-J. Kim and Y. Kim, *CrystEngComm*, 2016, **18**, 345-368.
  - 4 D. Feng, Z.-Y. Gu, Y.-P. Chen, J. Park, Z. Wei, Y. Sun, M. Bosch, S. Yuan and H.-C. Zhou, *J. Am. Chem. Soc.*, 2014, **136**, 17714-17717.
  - 5 W. Morris, B. Voloskiy, S. Demir, F. G  ndara, P.L. McGrier, H. Furukawa, D. Cascio, J.F. Stoddart and O.M. Yaghi, *Inorg. Chem.*, 2012, **51**, 6443-6445.
  - 6 W. Kraus and G. Nolze, *PowderCell 2.4*.
  - 7 *Materials Studio v4.3*, Accelrys: San Diego, U.S.A.; Cambridge, UK; Tokio, Japan, 2008.
  - 8 G. Socrates, “Infrared and Raman Characteristic Group Frequencies”, Wiley-VCH, Weinheim, 2004.
  - 9 P.R. Boyce, “Human Factors in Lighting”, CRC Press, Third Edition, 2014.
  - 10 S.K. Shevell, “The Science of Color”, Elsevier Science, Amsterdam, 2003.
  - 11 K.M.M. Krishna Prasad, S. Raheem, P. Vijayalekshmi, C. Kamala Sastri, *Talanta* 1996, **43**, 1187-1206.